MNRAS Advance Access published September 12, 2016

Reionisation in sterile neutrino cosmologies

Sownak Bose[1⋆], Carlos S. Frenk[1], Jun Hou[1], Cedric G. Lacey[1] and Mark R. Lovell[2,3]
[1]*Institute for Computational Cosmology, Durham University, South Road, Durham, UK, DH1 3LE*
[2]*GRAPPA Institute, Universiteit van Amsterdam, Science Park 904, 1098 XH Amsterdam, The Netherlands*
[3]*Instituut-Lorentz for Theoretical Physics, Niels Bohrweg 2, NL-2333 CA Leiden, The Netherlands*

10 September 2016

ABSTRACT
We investigate the process of reionisation in a model in which the dark matter is a warm elementary particle such as a sterile neutrino. We focus on models that are consistent with the dark matter decay interpretation of the recently detected line at 3.5 keV in the X-ray spectra of galaxies and clusters. In warm dark matter models the primordial spectrum of density perturbations has a cut-off on the scale of dwarf galaxies. Structure formation therefore begins later than in the standard cold dark matter (CDM) model and very few objects form below the cut-off mass scale. To calculate the number of ionising photons, we use the Durham semi-analytic model of galaxy formation, GALFORM. We find that even the most extreme 7 keV sterile neutrino we consider is able to reionise the Universe early enough to be compatible with the bounds on the epoch of reionisation from *Planck*. This, perhaps surprising, result arises from the rapid build-up of high redshift galaxies in the sterile neutrino models which is also reflected in a faster evolution of their far-UV luminosity function between $10 > z > 7$ than in CDM. The dominant sources of ionising photons are systematically more massive in the sterile neutrino models than in CDM. As a consistency check on the models, we calculate the present-day luminosity function of satellites of Milky Way-like galaxies. When the satellites recently discovered in the DES survey are taken into account, strong constraints are placed on viable sterile neutrino models.

Key words: cosmology: dark matter – galaxies: high-redshift – galaxies: evolution

1 INTRODUCTION

Dark matter, the non-baryonic component that makes up the majority of the mass of the Universe, is the foundation of today's cosmological paradigm. The standard model, ΛCDM, assumes that the dark matter is a cold, collisionless particle and that the energy density of the Universe today is dominated by dark energy in the form of a cosmological constant. This model has predictive power and accounts for basic measurements of the evolution of large-scale structure in our Universe, from the temperature anisotropies in the cosmic microwave background radiation (CMB) at early times (Ade et al. 2015), to the statistics of the galaxy clustering pattern today (e.g., Cole et al. 2005; Eisenstein et al. 2005; Zehavi et al. 2011). Its main shortcoming at present is that the cold particles have not yet been conclusively detected (but see Hooper & Goodenough 2011).

Cold particles are not the only well-motivated candidates for the dark matter. An example of a different kind of particle is the *sterile neutrino* (Dodelson & Widrow 1994; Abazajian et al. 2001a,b; Dolgov & Hansen 2002), which appears in a simple extension of the Standard Model. Its interaction with active neutrinos could source neutrino flavour oscillations. In order simultaneously to account for the dark matter and flavour oscillations, *at least* three right-handed sterile neutrinos are needed (Asaka & Shaposhnikov 2005; Asaka et al. 2007; Canetti et al. 2013). In this 'Neutrino Minimal Standard Model' (or νMSM), two of the sterile neutrinos interact more strongly with the active neutrinos than the third, which behaves as dark matter (Boyarsky et al. 2009b). With the appropriate choice of parameters in the Lagrangian, it is possible to obtain the correct dark matter density in sterile neutrinos.

Interest in νMSM has been boosted recently by the detection of an X-ray line at 3.5 keV in the stacked spectrum of galaxy clusters (Bulbul et al. 2014), M31 and the Perseus cluster (Boyarsky et al. 2014). According to these authors, the excess at 3.5 keV cannot be explained by any known metal lines and could, in fact, be the result of the decay of sterile neutrinos with a rest mass of 7 keV. This interpretation of the line has subsequently been challenged by several authors (see, for example, Riemer-Sorensen 2014; Malyshev et al. 2014; Jeltema & Profumo 2015b; Anderson et al. 2015). Most recently, Jeltema & Profumo (2015a) failed to detect any excess at 3.5 keV in a deep *XMM-Newton* observation of the dwarf spheroidal galaxy Draco, attributing the original line detection to an excitation of K VIII. Crucially, however, the Jeltema & Profumo (2015a) analysis made use of only a subset of the data; with the complete dataset and an alternative model for the backgrounds, Ruchayskiy et al. (2015) detected positive residuals at 3.5 keV at 2.3σ significance, with a flux consistent with those obtained from the original stacked galaxy cluster

⋆ E-mail: sownak.bose@durham.ac.uk

and M31 observations. Future X-ray observatories may establish the true identity of this line.

From the point of view of cosmology, the defining property of keV mass sterile neutrinos is that they behave as *warm dark matter* (WDM). In contrast to CDM, warm particles are kinematically energetic at early times and thus free stream out of small-scale primordial perturbations, inducing a cut-off in the power spectrum of density fluctuations. On large scales unaffected by the free streaming cut-off, structure formation is very similar in CDM and sterile neutrino cosmologies (and in WDM in general), but on scales comparable to or smaller than the cut-off, structure formation proceeds in a fundamentally different way in the two cases. No haloes form below a certain mass scale determined by the cut-off and the formation of small haloes above the cut-off is delayed (see Colín et al. 2000; Bode et al. 2001; Avila-Reese et al. 2001; Viel et al. 2005; Lovell et al. 2012; Schneider et al. 2012; Bose et al. 2016b,a)

For a 7 keV sterile neutrino, the cut-off mass is $\sim 10^9 M_\odot$. Thus, potentially observable differences from CDM would emerge on subgalactic scales and at high redshifts when the delayed onset of structure formation might become apparent. The Local Group and the early Universe are thus good hunting grounds for tell-tale signs that might distinguish warm from cold dark matter. There is now a wealth of observational data for small galaxies in the Local Group (e.g. Koposov et al. 2008; McConnachie 2012), as well as measurements of the abundance of galaxies at high redshifts (e.g. McLure et al. 2013; Bouwens et al. 2015) and estimates of the redshift of reionisation (Ade et al. 2015). One might hope that these data could constrain the parameters of WDM models (e.g. Schultz et al. 2014; Abazajian 2014; Calura et al. 2014; Dayal et al. 2015a,b; Governato et al. 2015; Lovell et al. 2015; Maio & Viel 2015; Bozek et al. 2016).

In this work, we address these questions using the Durham semi-analytic model of galaxy formation, GALFORM (Cole et al. 2000; Lacey et al. 2015), applied both to CDM and sterile neutrino dark matter. The model follows the formation of galaxies in detail using a Monte Carlo technique for calculating halo merger trees and well-tested models for the baryon physics that result in the formation of visible galaxies. GALFORM predicts the properties of the galaxy population at all times. This approach has the advantage that it can easily generate large statistical samples of galaxies at high resolution for a variety of dark matter models which would be prohibitive in terms of computational time with the current generation of hydrodynamic simulations.

This paper is structured as follows. In Section 2 we introduce the concept of sterile neutrinos and the models considered in this paper. In Section 3 we describe the astrophysical motivation behind this work, as well as the semi-analytic model, GALFORM, used in our analysis. Our results are presented in Section 4 and our main conclusions summarised in Section 5.

2 THE STERILE NEUTRINO MODEL

Sterile neutrinos[1] are relativistic when they decouple and therefore have non-negligible velocities which smear out density perturbations on small scales. Hence, sterile neutrinos behave as WDM. In the original model introduced by Dodelson & Widrow (1994), sterile neutrinos are created by non-resonant mixing with active neutrinos in the Standard Model. The scale of the free streaming is determined solely by the rest mass of the sterile neutrino – the lighter the particle, the larger the free streaming length, and the larger the scales at which differences relative to CDM appear.

Shi & Fuller (1999) proposed an alternative production mechanism in which the abundance of sterile neutrinos is boosted by a primordial *lepton asymmetry*. The value of this quantity, which measures the excess of leptons over anti-leptons, affects the scale of free streaming in addition to the rest mass of the sterile neutrino. Asaka & Shaposhnikov (2005) proposed a model for the generation of the lepton asymmetry by introducing three right-handed sterile neutrinos in what is known as the 'Neutrino Minimal Standard Model' (νMSM, see also Boyarsky et al. 2009b). In this model, a keV mass sterile neutrino (labelled N_1) is partnered with two GeV mass sterile neutrinos (N_2 and N_3). It is N_1 that behaves as the dark matter, with its keV mass (M_1) leading to early free streaming. The decay of N_2 and N_3 prior to the production of N_1 generates significant lepton asymmetry; this boosts the production of N_1 via resonant mixing. Here, we formally quantify the lepton asymmetry, or L_6, as:

$$L_6 \equiv 10^6 \left(\frac{n_{\nu_e} - n_{\bar{\nu_e}}}{s} \right) , \quad (1)$$

where n_{ν_e} is the number density of electron neutrinos, $n_{\bar{\nu}_e}$ the number density of electron anti-neutrinos and s is the entropy density of the Universe (Laine & Shaposhnikov 2008).

A third parameter in the νMSM is the *mixing angle*, θ_1. The requirement that the model should achieve the correct dark matter abundance for a given sterile neutrino rest mass uniquely fixes the value of θ_1 for a particular choice of L_6. The X-ray flux, F, associated with the decay of N_1 is then proportional to $\sin^2(2\theta_1) M_1^5$. We refer the reader to Venumadhav et al. (2015) and Lovell et al. (2015) for a more comprehensive discussion of the sterile neutrino model.

In this paper we are particularly interested in sterile neutrinos that could decay to produce two 3.5 keV photons. We therefore fix the mass $M_1 = 7\,\mathrm{keV}$. At this mass, the 'warmest' and 'coldest' sterile neutrino models that achieve the correct dark matter density correspond to $L_6 = 700$ and $L_6 = 8$ respectively. By this we mean that the $L_6 = 700$ model exhibits deviations from CDM at larger mass scales than the $L_6 = 8$ model, which produces similar structure to CDM down to the scale of dwarf galaxies.

For the $L_6 = 700$ case, however, the corresponding mixing angle (which we remind the reader is now *fixed*) does not lead to the X-ray decay flux required to account for the observations of Bulbul et al. (2014) and Boyarsky et al. (2014). For this reason, we additionally consider the case $L_6 = 12$, which corresponds to the warmest 7 keV sterile neutrino model that has the correct dark matter abundance *and* produces the correct flux at 3.5 keV. This information is summarised in Table 1. Here, we also quote a characteristic wavenumber, $k_{1/4}$, which measures the scale at which the linear power spectrum for a given L_6 has $1/4$ of the power of the CDM linear power spectrum. This parameter characterises the 'warmth' of the model. The most extreme case ($L_6 = 700$) has $k_{1/4} = 16.05\ h/\mathrm{Mpc}$, whereas the model closest to CDM ($L_6 = 8$) has $k_{1/4} = 44.14\ h/\mathrm{Mpc}$.

Fig. 1 shows the linear power spectrum (in arbitrary units) of these three models ($L_6 = (8, 12, 700)$), with the CDM power spectrum also plotted for comparison. The power spectra for the sterile neutrino models were computed by first calculating the momentum distribution functions for these models using the methods outlined by Laine & Shaposhnikov (2008) and Ghiglieri & Laine (2015), and using these to solve the Boltzmann

[1] These particles are 'sterile' in the sense that they do not interact via the weak force, as is the case for active neutrinos in the Standard Model.

equation with a modified version of the CAMB code (Lewis et al. 2000; Boyarsky et al. 2009a,c; Lovell et al. 2015). The cosmological parameters assumed are those derived from Ade et al. (2015): $\Omega_m = 0.307$, $\Omega_\Lambda = 0.693$, $\Omega_b = 0.0483$, $h = 0.678$, $\sigma_8 = 0.823$, and $n_s = 0.961$. The most striking feature is how, for the same 7 keV sterile neutrino, the scale of the cut-off (as measured by, say, $k_{1/4}$) changes with L_6. The cutoff in the $L_6 = 8$ power spectrum occurs at a similar scale to that introduced by a 3.3 keV thermal relic, which, at 95% confidence, is the lower limit on the WDM particle mass set by constraints from the Lyman-α forest (Viel et al. 2013, although see Baur et al. 2015 for a revised lower limit). The $L_6 = 12$ case is therefore in tension with the lower limits from the Lyman-α forest, but it should be noted that the derived lower limits are sensitive to assumptions made for the thermal history of the IGM (Garzilli et al. 2015).

The truncated power spectra in the three sterile neutrino models results in a suppression in the abundance of haloes (and by extension, the galaxies in them) at different mass scales in the different models. This is illustrated in Fig. 2 where we show the $z = 0$ halo mass functions for CDM and for $L_6 = (8, 12, 700)$, as predicted by the ellipsoidal collapse formalism of Sheth & Tormen (1999). In this model, the number density of haloes within a logarithmic interval in mass ($\mathrm{d}n/\mathrm{d}\log \mathrm{M_{halo}}$) is quantified by:

$$\frac{\mathrm{d}n}{\mathrm{d}\log M_{\rm halo}} = \frac{\bar{\rho}}{M_{\rm halo}} f(\nu) \left| \frac{\mathrm{d}\log \sigma^{-1}}{\mathrm{d}\log M_{\rm halo}} \right| , \qquad (2)$$

where $\bar{\rho}$ is the mean matter density of the Universe, $\nu = \delta_c/\sigma(M_{\rm halo})$, $\delta_c = 1.686$ is the density threshold required for collapse and $\sigma(M_{\rm halo})$ is the variance of the density field, smoothed at a scale, $M_{\rm halo}$ (see Section 3.3). In the ellipsoidal collapse model the multiplicity function, $f(\nu)$, takes the form:

$$f(\nu) = A\sqrt{\frac{2q\nu}{\pi}} \left[1 + (q\nu)^{-p}\right] e^{-q\nu/2}, \qquad (3)$$

where $A = 0.3222$, $q = 0.707$ and $p = 0.3$. Fig. 2 shows how the mass functions in the sterile neutrino models peel off from CDM at different mass scales directly related to $k_{1/4}$. The halo masses corresponding to these wavenumbers can be estimated by:

$$M_{1/4} = \frac{4}{3}\pi\bar{\rho}\left(\frac{\pi}{k_{\rm hm}}\right)^3 , \qquad (4)$$

giving $M_{1/4} = \left(1.1 \times 10^8, 7.8 \times 10^8, 2.3 \times 10^9\right)\ h^{-1}\ M_\odot$ for $L_6 = (8, 12, 700)$ respectively. Clearly, the largest suppression in halo abundance relative to CDM occurs for the $L_6 = 700$ case, and the least for the $L_6 = 8$ case, consistent with our discussion of the significance of the characteristic scale $k_{1/4}$. For example, at $z = 0$, there are half as many $\sim 10^8\ h^{-1}\ M_\odot$ in $L_6 = 8$ as in CDM. By comparison, there are ~ 150 times fewer haloes at the same mass scale for $L_6 = 700$ relative to CDM. The $L_6 = 12$ model lies in between these two cases, producing ~ 20 times fewer haloes of $10^8\ h^{-1}\ M_\odot$.

3 GALAXY FORMATION

We begin by discussing the astrophysical quantities and observables that we will use to constrain sterile neutrino models. We then briefly introduce the semi-analytic model of galaxy formation, GALFORM, that we will use to predict these quantities for both CDM and sterile neutrino models. We build upon the ideas and methods laid out by Hou et al. (2015, hereafter Hou15).

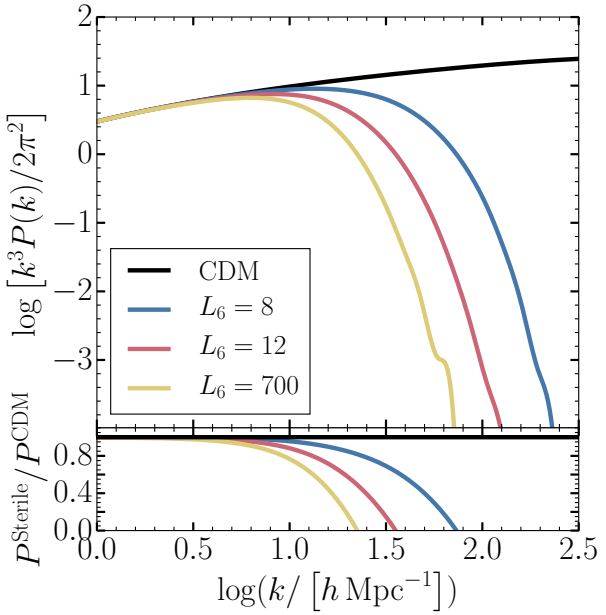

Figure 1. *Top panel:* The dimensionless matter power spectra for the different dark matter candidates considered in this paper. In addition to CDM, we consider a 7 keV sterile neutrino with three values of $L_6 = (8, 12, 700)$, shown with the colours indicated in the legend. For the same sterile neutrino mass, different L_6 values lead to deviations from CDM on different scales, with the most extreme case being the $L_6 = 700$ model. *Bottom panel*: The ratio of each power spectrum to that of CDM.

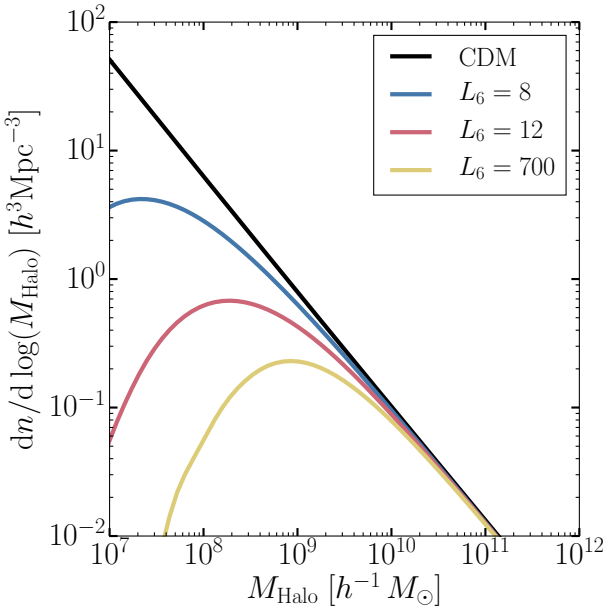

Figure 2. The $z = 0$ halo mass functions for CDM and 7.5 keV sterile neutrino models with leptogenesis parameter, $L_6 = (8, 12, 700)$, as predicted by the ellipsoidal collapse model of Sheth & Tormen 1999, calculated using Eqs. 2 & 3. The different cut-off scales for the sterile neutrino power spectra in Fig. 1 are reflected in the different mass scales at which the corresponding halo mass functions are suppressed below the CDM mass function.

Table 1. Properties of the four dark matter models studied in this paper: CDM and 7 keV sterile neutrino models with lepton asymmetry, $L_6 = (8, 12, 700)$. The quantity $k_{1/4}$ is the wavenumber at which the amplitude of the power spectrum is $1/4$ that of the CDM amplitude; it is a measure of the "warmth" of the model. The last three columns indicate whether the model gives (1) the correct dark matter density; (2) whether the particle can decay to produce a line at 3.5 keV; and (3) whether the corresponding mixing angle can produce an X-ray decay flux consistent with the observations of Boyarsky et al. 2014; Bulbul et al. 2014.

Model; L_6	$k_{1/4}$ $[h/\mathrm{Mpc}]$	Right DM abundance?	Decay at 3.5 keV?	Flux consistent with 3.5 keV X-ray line?
CDM; –	–	✓	✗	✗
7 keV; 8	44.14	✓	✓	✓
7 keV; 12	23.27	✓	✓	✓
7 keV; 700	16.05	✓	✓	✗

3.1 A galactic "tug-of-war"

One of the most important physical processes involved in galaxy formation is supernova feedback (SNfb). By ejecting cold gas from galaxies, SNfb regulates star formation, inhibiting galaxy formation in small mass haloes (Larson 1974; White & Frenk 1991). SNfb is thought to be responsible for the relatively flat galaxy stellar mass and luminosity functions compared to the steeply rising halo mass function predicted by N-body simulations for ΛCDM (e.g. Jenkins et al. 2001; Tinker et al. 2008; Kauffmann et al. 1993; Cole et al. 1994). On the smallest scales, SNfb, in conjunction with photoionisation of gas in the early Universe, can explain the small number of faint satellite galaxies seen around galaxies like the Milky Way in this model (Efstathiou 1992; Benson et al. 2003; Sawala et al. 2015).

Unless AGN contribute a significant number of ionising photons (Madau & Haardt 2015; Khaire et al. 2016), SNfb cannot be so strong as to suppress the production of ionising photons at high redshift required to reionise the Universe by $z \sim 6$, as inferred from QSO absorption lines (Mitra et al. 2015; Robertson et al. 2015) and the microwave background data (Ade et al. 2015). Thus, at least in CDM, the small observed number of faint galaxies sets a lower limit to the strength of feedback, while the requirement that the Universe be ionised early enough sets an upper limit. Hou et al. (2015) found that the simple models of SNfb usually assumed in semi-analytic models of galaxy formation do not satisfy both these requirements. They proposed instead a more complicated model in which the strength of SNfb evolves in redshift, as suggested by the SNfb model of Lagos et al. (2013) (see Section 3.2 below).

Since in WDM the number of small haloes is naturally suppressed, for a model to be viable, SNfb must be weak enough so that there are enough ionising photons at high redshift, as well as a sufficient number of satellite galaxies to account for observations.

3.2 Supernova feedback in GALFORM

The Durham semi-analytic model of galaxy formation, GALFORM, was introduced by Cole et al. (2000) and has been upgraded regularly as our understanding of the physical processes involved in galaxy formation improves and better observational constraints are obtained. For example, Baugh et al. (2005) introduced a top-heavy IMF in bursts, Bower et al. (2006) introduced AGN feedback and Lagos et al. (2011) introduced a star formation law that depends on the molecular gas content of the ISM. The most recent version of the model Lacey et al. (2015) includes all of these revisions.

The observational data normally used to constrain and test semi-analytic models includes galaxies with stellar mass, $M_\star \gtrsim 10^8 \mathrm{M}_\odot$. When attempting to extend the Lacey et al. (2015) model to lower mass galaxies, Hou et al. (2015) found that the original prescription for SNfb had to be modified as discussed in Section 3.1. In the original prescription, the mass loading factor, β, defined as the ratio of the mass ejection rate to the star formation rate, is assumed to be a power law in the circular velocity, $V_{\rm circ}$, of the galaxy. To match the observed satellite luminosity function and produce an acceptable metallicity-luminosity relation for Milky Way satellites, Hou15 required a mass loading factor given by a broken power law with a redshift dependence:

$$\beta = \begin{cases} (\mathrm{V_{circ}}/\mathrm{V_{SN}})^{-\gamma_{\rm SN}} & \mathrm{V_{circ}} \geqslant \mathrm{V_{thresh}} \\ (\mathrm{V_{circ}}/\mathrm{V'_{SN}})^{-\gamma'_{\rm SN}} & \mathrm{V_{circ}} < \mathrm{V_{thresh}}, \end{cases} \quad (5)$$

where $\mathrm{V'_{SN}}$ is chosen such that the two power laws in Eq. 5 join at $\mathrm{V_{circ}} = \mathrm{V_{thresh}}$, $\gamma_{\rm SN} = 3.2$, $\gamma'_{\rm SN} = 1.0$, $\mathrm{V_{thresh}} = 50\,\mathrm{kms}^{-1}$ and:

$$\mathrm{V_{SN}} = \begin{cases} 180 & z > 8 \\ -35z + 460 & 4 \leqslant z \leqslant 8 \\ 320 & z < 4 \end{cases}. \quad (6)$$

This redshift dependence is chosen to capture the overall behaviour of Lagos et al. (2013) supernova feedback model. In the Hou et al. (2015) model, the feedback strength is assumed to be the same as in Lacey et al. (2015) at $z < 4$, but is weaker at higher redshifts and in galaxies with $\mathrm{V_{circ}} < \mathrm{V_{thresh}} = 50\,\mathrm{kms}^{-1}$. We will refer to this feedback scheme as the 'EvoFb' (evolving feedback) model.

The values of $\gamma_{\rm SN}$ and $\mathrm{V_{thresh}}$ in this model were calibrated for CDM and need to be recalibrated for the sterile neutrino models that we are considering. We find that the values $\gamma_{\rm SN} = 2.6$ for $L_6 = 700$, $\gamma_{\rm SN} = 2.8$ for $L_6 = (8, 12)$ and $\mathrm{V_{thresh}} = 30\,\mathrm{kms}^{-1}$ for all three values of L_6 provide the best-fit to the local b_J and K-band luminosity functions, the primary observables used to calibrate GALFORM.

3.3 Halo merger trees with sterile neutrinos

We generate merger trees using the extension of the Cole et al. (2000) Monte Carlo technique (based on the extended Press-Schechter (EPS) theory) described in Parkinson et al. (2008). In models in which the linear power spectrum, $P(k)$, has a cut-off, as in our sterile neutrino models, a small correction is required to the EPS formalism: to obtain the variance of the density field,

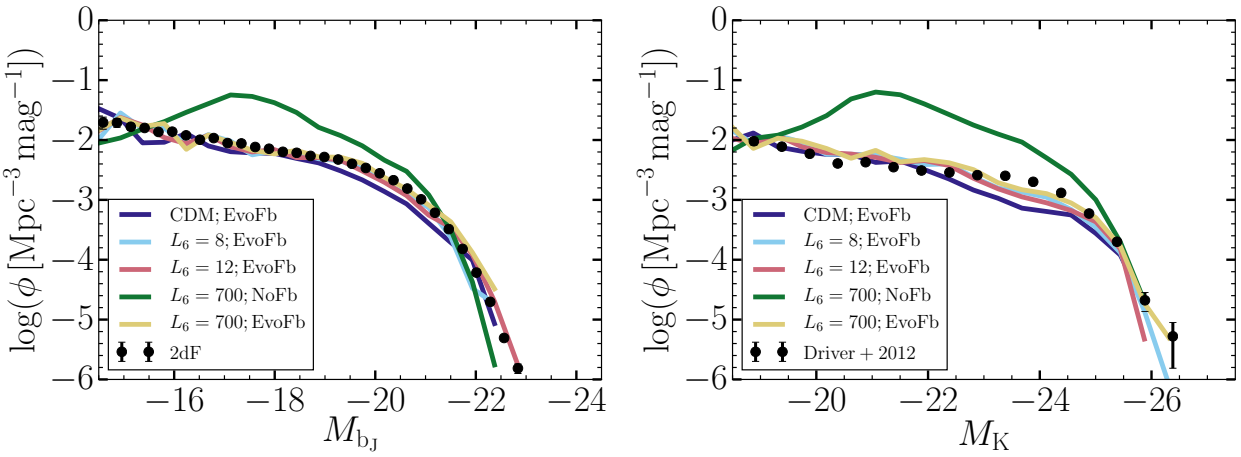

Figure 3. The $z = 0$ field galaxy luminosity functions in the b_J-band (left panel) and the K-band (right panel) for the four dark matter models considered in this paper: CDM and 7 keV sterile neutrino models with $L_6 = (8, 12, 700)$. The evolving feedback (EvoFb) model is used in GALFORM. For the $L_6 = 700$ case, we also show an extreme model in which the feedback has been completely turned off ('NoFb'). The black points are observational estimates (Norberg et al. 2002; Driver et al. 2012).

$\sigma(M_{\rm halo})$, $P(k)$ needs to be convolved with a sharp k-space filter rather than with the real-space top-hat filter used for CDM (Benson et al. 2013). This choice results in good agreement with the conditional halo mass function obtained in N-body simulations (see, for example, Fig. 6 in Lovell et al. 2015).

Using our Monte Carlo technique rather than N-body simulations to generate merger trees has the advantage that different sterile neutrino models can be studied at minimum computational expense while avoiding the complication of spurious fragmentation in filaments that occurs in N-body simulations with a resolved cut-off in $P(k)$ (e.g. Wang & White 2007; Lovell et al. 2014).

4 RESULTS

In this section, we present the main results of our models, consisting of predictions for field and satellite luminosity functions and the redshift of reionisation. We also investigate the sources that produce the ionising photons at high redshift.

4.1 Field luminosity functions

As discussed in Section 3.2, the parameters of the SNfb model in GALFORM were calibrated so as to obtain a good match to the present-day field galaxy luminosity functions. The b_J and K-band luminosity function in CDM and the $L_6 = (8, 12, 700)$ 7 keV sterile neutrino models are shown in Fig. 3. In both cases we have made use of the EvoFb feedback scheme of Section 3.2. We also consider an extreme model for $L_6 = 700$, in which supernova feedback is turned off completely ('NoFb'), thus maximising the amount of gas that is converted into stars.

In Fig. 3 we see that with the EvoFb scheme the observed luminosity functions are well reproduced in CDM and all our sterile neutrino models. This should come as no surprise since the EvoFb model parameters were tuned to match these particular data. As mentioned in Section 2, the $L_6 = 700$ model, while inconsistent with the 3.5 keV line (see Table 1), is interesting because it has the most extreme power spectrum cut-off for a 7 keV sterile neutrino that produces the correct dark matter abundance. The maximum star formation efficiency in any model is obtained by turning off SNfb altogether. If in this limiting scenario the $L_6 = 700$ model produces too few faint galaxies to match the field luminosity function, this extreme model would be strongly ruled out. As Fig. 3 shows, the resultant luminosity function (shown in green) in fact overproduces faint galaxies.

4.2 Redshift of reionisation

Since the onset of halo formation occurs later in sterile neutrino models compared to CDM (e.g. Bose et al. 2016b), star formation in dwarf galaxies is delayed (e.g. Colín et al. 2015; Governato et al. 2015). Since, in addition, there are no haloes below a cut-off mass, it is unclear that enough sources of ionising photons will have formed to ionise hydrogen early enough to be consistent with the *Planck* limits on the redshift of reionisation (Ade et al. 2015).

To answer this question we use GALFORM to calculate the ratio of the comoving number density of ionising photons produced, n_γ, to that of hydrogen nuclei, $n_{\rm H}$ as:

$$\mathcal{R}(z) = \frac{n_\gamma}{n_{\rm H}} = \frac{\int_z^\infty \epsilon(z')\,{\rm d}z'}{n_{\rm H}}, \qquad (7)$$

where $\epsilon(z')$ is the comoving number density of Lyman continuum photons produced per unit redshift. The Universe is deemed to be fully ionised at redshift $z_{\rm reion}^{\rm full}$ when the ratio in Eq. 7 reaches the value:

$$\mathcal{R}(z)|_{\rm full} = \frac{1 + N_{\rm rec}}{f_{\rm esc}} = 6.25. \qquad (8)$$

Here $N_{\rm rec}$ is the number of recombinations per hydrogen atom and $f_{\rm esc}$ is the fraction of ionising photons that are able to escape a galaxy into the IGM. Raičević et al. (2011) advocate a value of $N_{\rm rec} = 1$ based on the hydrodynamical simulations of Iliev et al. (2006) and Trac & Cen (2007). Finlator et al. (2012) suggest that photoheating would smooth the diffuse IGM and reduce the clumping factor by a factor of three compared with the value derived by Iliev et al. (2006). In this work, we will adopt a value $N_{\rm rec} = 0.25$

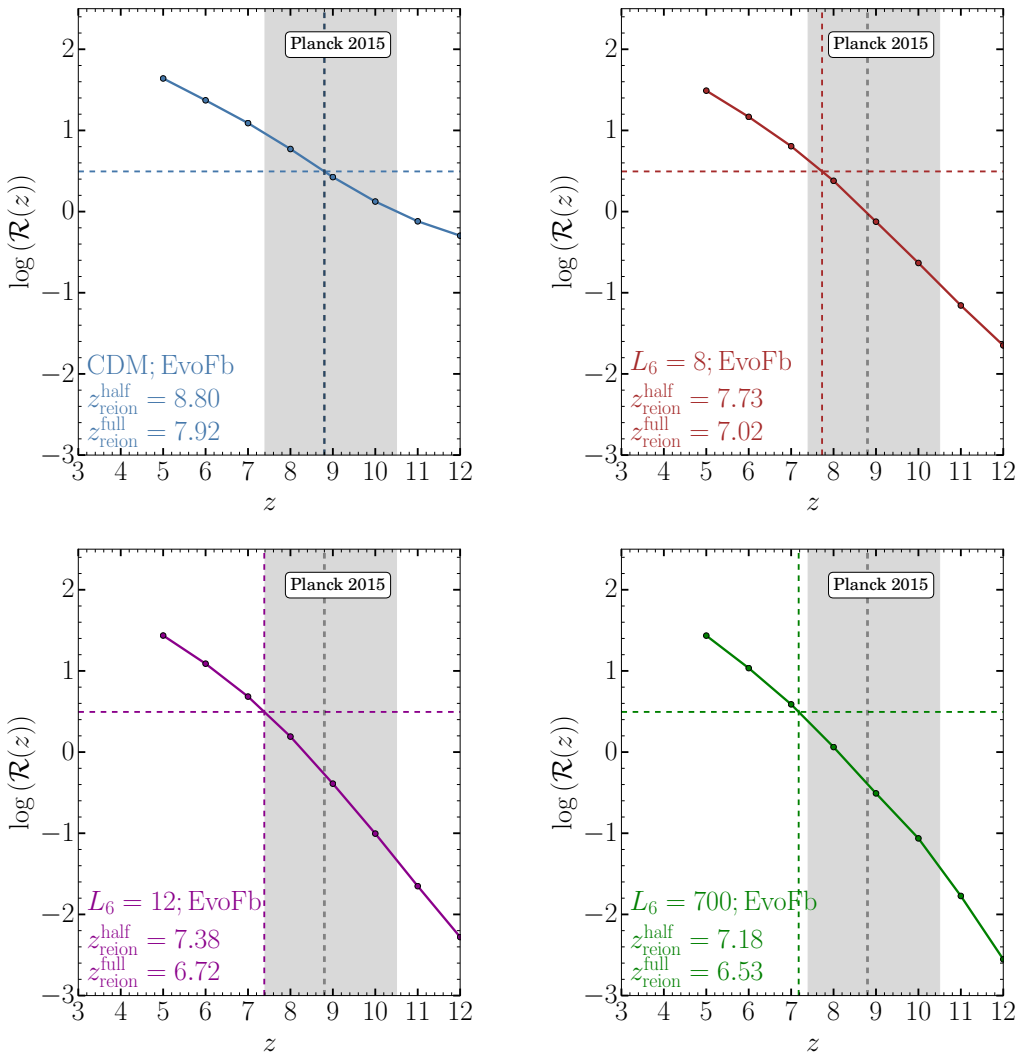

Figure 4. The ratio of the total number of ionising photons produced up to redshift z as a fraction of the total comoving number density of hydrogen nuclei (solid lines in each panel). In each panel, we show the predictions for the different dark matter models under the EvoFb scheme. The intersection of the coloured dashed lines marks the redshift at which the Universe is 50% ionised; the redshifts for 50% ($z_{\rm reion}^{\rm half}$) and 100% reionisation ($z_{\rm reion}^{\rm full}$) are listed in the bottom left of each panel. The dashed grey line and shaded grey region demarcate the observational constraints as obtained from the *Planck* satellite, $z_{\rm reion}^{\rm half} = 8.8^{+1.7}_{-1.4}$ (at 68% confidence).

(as in Hou15), but we have checked that our conclusions are insensitive to the exact value of this parameter. Furthermore, we assume $f_{\rm esc} = 0.2$, which is consistent with the value used by Raičević et al. (2011). Sharma et al. (2016) present observational and theoretical evidence in support of this choice of $f_{\rm esc}$ (see also Khaire et al. 2016).

The microwave background data measure the optical depth to the time when the Universe (re)combined. This is usually converted into an equivalent 'redshift of reionisation' assuming a model of non-instantaneous reionisation. The value quoted in Ade et al. (2015) corresponds to $z_{\rm reion}^{\rm half}$, the redshift at which the Universe is *half* ionised. With our assumptions this corresponds to:

$$\mathcal{R}(z)|_{\rm half} = 3.125. \quad (9)$$

Reionisation suppresses galaxy formation in low mass haloes through an effect known as photoionisation feedback. In GALFORM, this is modelled using the approximation described in Benson et al. (2003): for haloes with virial velocity $V_{\rm vir} < V_{\rm crit}$, no gas cooling takes place for $z < z_{\rm crit}$. As in Hou15, we adopt $z_{\rm crit} = z_{\rm reion}^{\rm full}$ and $V_{\rm crit} = 30\,{\rm km s}^{-1}$ (Okamoto et al. 2008).

In the standard Lacey et al. (2015) prescription, SNfb is modelled as a power law in the circular velocity of the galaxy without any dependence on redshift. Hou15 found that this model predicts $z_{\rm reion}^{\rm half} = 6.1$ for CDM, in conflict with the bounds by Ade et al. (2015): $z_{\rm reion}^{\rm half} = 8.8^{+1.7}_{-1.4}$. We expect that sterile neutrino models, in which the formation of galaxies is both suppressed and delayed, would be in even greater conflict with the *Planck* observations. For this reason, in what follows we only consider the predictions of the evolving feedback (EvoFb) model of Hou15 (Section 3.2) which, at least for CDM, predicts an acceptable value for $z_{\rm reion}^{\rm half}$.

Fig. 4 shows the evolution of $\mathcal{R}(z)$ with redshift for CDM and sterile neutrino models with $L_6 = (8, 12, 700)$ according to GALFORM with EvoFb feedback. In each panel, the intersection of the colour dashed lines marks $z_{\rm reion}^{\rm half}$, where $n_\gamma/n_{\rm H} = 3.125$. The dashed grey line and shaded grey region mark the median and 68%

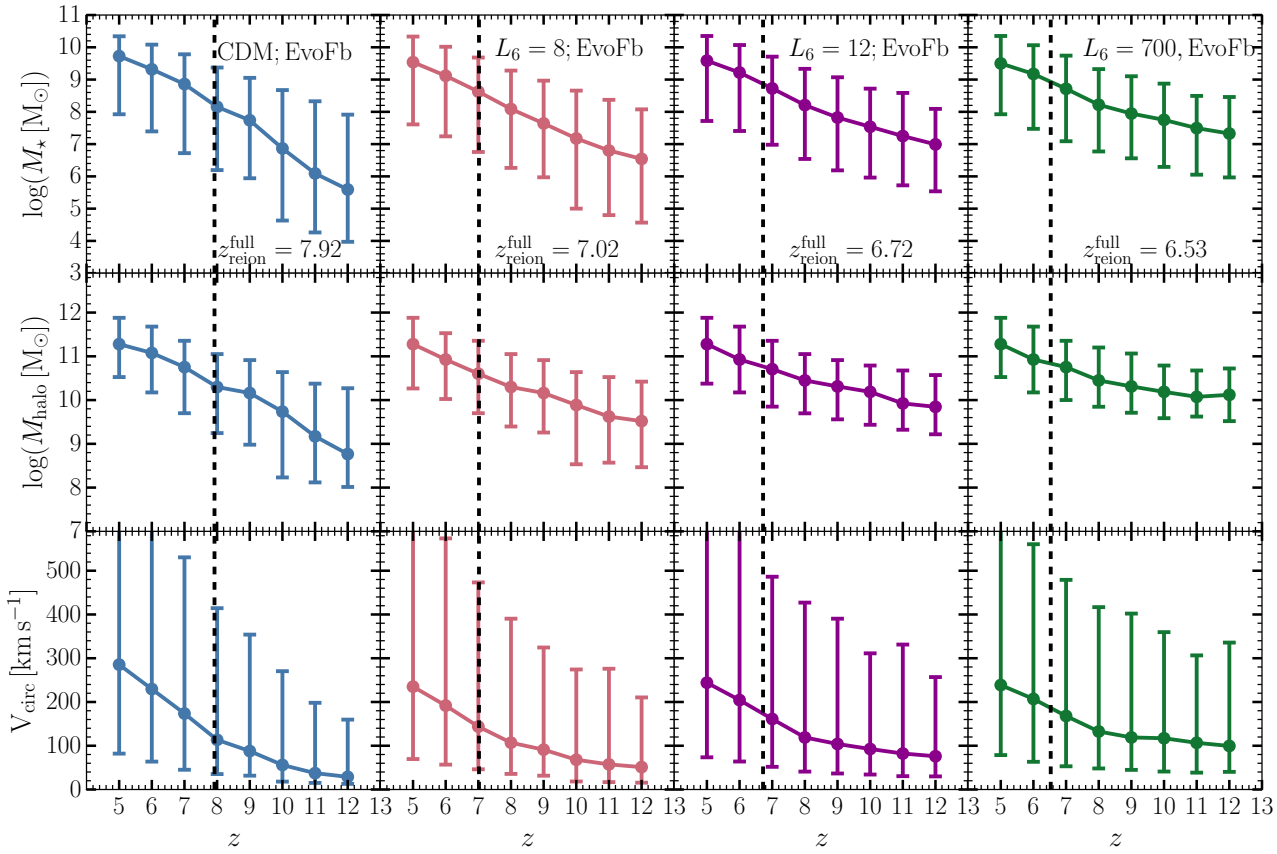

Figure 5. Properties of the sources that produce ionising photons as a function of redshift for CDM and 7 keV sterile neutrino models with $L_6 = (8, 12, 700)$. The properties shown are stellar mass, $M_\star$ (top row), halo mass $M_{\rm halo}$ (middle row) and circular velocity ($\rm V_{circ}$). The median (solid lines), 5th and 95th percentiles (error bars) are determined by weighting the contribution of each galaxy to the total ionising emissivity at that redshift. The black vertical dashed line in each case marks the redshift at which the Universe is half ionised.

confidence intervals from Ade et al. (2015): $z_{\rm reion}^{\rm half} = 8.8^{+1.7}_{-1.4}$. In the bottom left of each panel, we give $z_{\rm reion}^{\rm half}$ and $z_{\rm reion}^{\rm full}$ predicted for each model.

All three 7 keV sterile neutrino models have values of $z_{\rm reion}^{\rm half}$ that are broadly consistent with the *Planck* data. The $L_6 = (12, 700)$ models fall just outside the lower 68% confidence lower limit and the $L_6 = 8$ model just inside. This is a non-trivial result given the paucity of early structure in these models compared to CDM. Unsurprisingly, $z_{\rm reion}^{\rm half}$ is higher in CDM [2]. Fig. 4 already hints at the reason why the sterile neutrino models are able to ionise the Universe early enough. Comparing, for example, the $L_6 = 700$ model (bottom right panel) to CDM (top left panel), it is clear that the evolution of $\log(\mathcal{R}(z))$ is steeper in the former, that is more UV photons are produced per unit redshift in the $L_6 = 700$ case, even though the *total* number of photons at that redshift is larger in CDM. For $L_6 = 8$, the most 'CDM-like' sterile neutrino model, the gradient of $\log(\mathcal{R}(z))$ is shallower. We will return to this feature shortly.

4.3 The galaxies responsible for reionisation

We have seen that in spite of the delayed onset of galaxy formation, even the most extreme 7 keV sterile neutrino model is able to ionise the Universe early enough to be consistent with the constraints from *Planck*. To explore why this is so, we show in Fig. 5 several properties of the sources that contribute the bulk of the ionising photons at each redshift. Each column in the figure corresponds to a different dark matter model, while each row corresponds to a different property of the ionising sources: total stellar mass ($M_\star$, first row), halo mass ($M_{\rm halo}$, second row) and galaxy circular velocity ($\rm V_{circ}$, third row). The black vertical dashed lines mark $z_{\rm reion}^{\rm full}$, which is given in the top row in each case.

In CDM, the median stellar mass (i.e. the mass below which galaxies produce 50% of the ionising emissivity) at $z = z_{\rm reion}^{\rm full}$ is $\sim 10^8\,M_\odot$, whereas in the three sterile neutrino models the median mass is close to $\sim 10^9\,M_\odot$. The larger scatter in $M_\star$ and $M_{\rm halo}$ for CDM is due to the wide range of mass of the galaxies that

[2] We note that our results in this section contradict those by Rudakovskiy & Iakubovskyi (2016), who find that in the 7 keV $L_6 = 10$ model the Universe is reionised *earlier* than in CDM. This is ascribed to the lack of 'mini'-haloes in the sterile neutrino cosmology, which reduces the average number of recombinations per hydrogen atom. In our analysis this amounts to a reduction in the value of $N_{\rm rec}$ in Eq. 8. However, we have checked that even reducing the value of $N_{\rm rec}$ by a factor of 10 does not affect our results significantly.

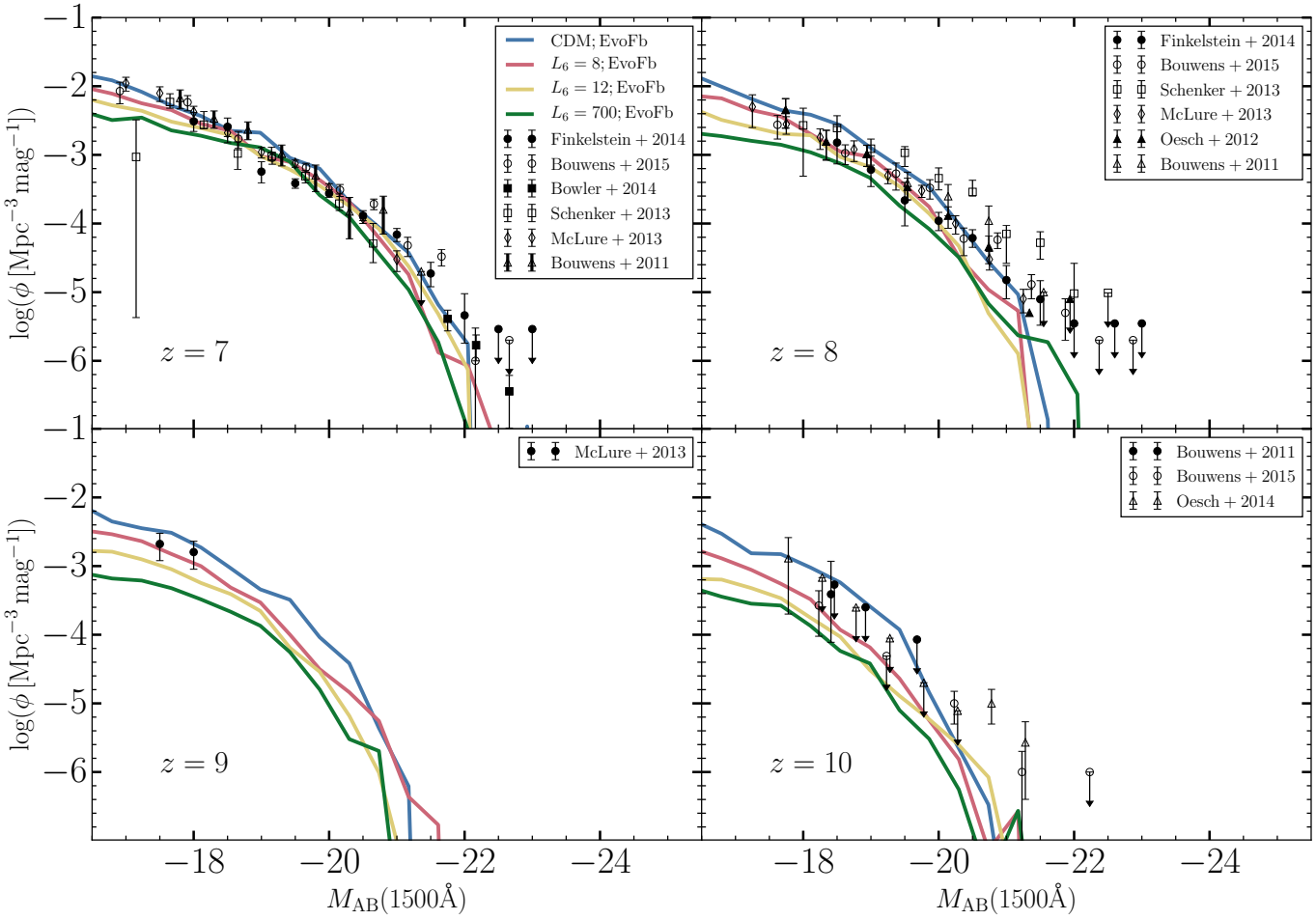

Figure 6. Evolution of the rest frame far-UV galaxy luminosity functions from $z = 7 - 10$ in our models. The predictions of GALFORM for CDM and the $L_6 = (8, 12, 700)$ 7 keV sterile neutrino models are shown with solid colour lines as indicated in the legend. The symbols with errorbars are observational measurements (Bouwens et al. 2011b,a; Oesch et al. 2012; Schenker et al. 2013; McLure et al. 2013; Finkelstein et al. 2014; Bowler et al. 2014; Oesch et al. 2014; Bouwens et al. 2015).

contribute to the ionising photon budget. For example, at $z = 10$, galaxies with mass in the range $10^4\,M_\odot < M_\star < 10^9\,M_\odot$ contribute 90% of the ionising photons, whereas in the $L_6 = (12, 700)$ models, 90% of the photons are produced by galaxies with mass in the range $10^6\,M_\odot < M_\star < 10^9\,M_\odot$ since very few galaxies with $M_\star < 10^6\,M_\odot$ form in these models. The result is that the primary sources of ionising photons at high redshift in sterile neutrino are on average *more massive* than in CDM.

The build-up of the galaxy population in our models is illustrated in Fig. 6 which shows the rest frame far-UV (1500 Å) luminosity functions at $z = 7, 8, 9, 10$ in CDM and the $L_6 = (8, 12, 700)$ models. As noted in Hou15, in CDM the EvoFb feedback model predicts luminosity functions that are in good agreement with the data at all redshifts. EvoFb underpredicts the abundance of the brightest galaxies ($M_{\mathrm{AB}}(1500\text{Å}) < -21$) for all dark matter models compared to the observations. For these galaxies, however, the data include many upper limits. Furthermore, these rare luminous galaxies are not the dominant sources of ionising photons (c.f. Fig. 5), so we do not expect the underprediction from the Hou15 model to impact our conclusions significantly for the redshift of reionisation in this paper. For $L_6 = (12, 700)$, the models also underpredict the abundance of galaxies fainter than $M_{\mathrm{AB}}(1500\text{Å}) \sim -20$ galaxies at $z = 9$ and $z = 10$. Reducing the strength of SNfb at $z > 8$ slightly can bring these models into agreement with the data without spoiling the agreement at $z = 0$.

An interesting feature of Fig. 6 is that while the $L_6 = (8, 12, 700)$ sterile neutrino models produce fewer galaxies fainter than $M_{\mathrm{AB}}(1500\text{Å}) \sim -20$ at $z = 10$, all three models catch up with CDM by $z = 7$, roughly the time by which 50% hydrogen reionisation has occurred. The *build-up of the high redshift galaxies therefore proceeds more rapidly* in the sterile neutrino cosmologies than in CDM. This is consistent with the behaviour of the rate of ionising photon production seen in Section 4.2, where the slope of $\log(n_\gamma/n_{\mathrm{H}})$ was shown to be steeper for sterile neutrino models compared to CDM.

The reason for the differing rates of galaxy formation at high redshift in the different models can be understood as follows. Due to the lack of progenitors below the cut-off mass scale, WDM haloes build up via roughly equal-mass mergers of intermediate mass haloes. Near the free streaming scale, the growth rate of haloes is therefore more rapid in WDM than in CDM (see, e.g. Ludlow et al. 2016). This is why soon after the formation of the

first galaxies the rate of galaxy formation in sterile neutrino models 'catches up' with the corresponding rate in CDM. This rapid early evolution, reflected for example in the UV luminosity function, is a generic prediction of WDM, independently of the details of the galaxy formation model.

4.4 Satellites of the Milky Way

The Milky Way satellite luminosity function has been used to set limits on the warm dark matter particle mass: if the power spectrum cut-off occurs on too large a scale, too few haloes form to account for the observed number of satellites (Macciò & Fontanot 2010; Polisensky & Ricotti 2011; Lovell et al. 2012; Nierenberg et al. 2013; Kennedy et al. 2014). These studies considered non-resonantly produced thermal relics (but see Schneider 2016). Lovell et al. (2015) considered sterile neutrino models, similar to ours, with different particle masses and values of L_6 and an earlier version of GALFORM (Gonzalez-Perez et al. 2014). There are degeneracies between the shape of the WDM power spectrum and some of the parameters of the galaxy formation model, particularly, of course, the strength of SNfb (see Kennedy et al. 2014 for a discussion). These degeneracies are mitigated in our case by considering a variety of observational constraints involving a range of halo masses and redshifts.

We have allowed the strength of SNfb to vary with redshift, by assuming that SNfb is weaker at high redshift. In Section 4.2, we found that this modification to the feedback scheme in GALFORM allows CDM and the $L_6 = (8, 12, 700)$ sterile neutrino models to reionise the Universe early enough to be consistent with the *Planck* limits on the redshift of reionisation. It is not clear, however, what the effect of reducing the strength of feedback will be on observables at lower redshifts. In particular, we expect the predicted luminosity function of satellites in the Milky Way to be particularly sensitive to this modification.

To predict the satellite luminosity functions around galaxies similar to the Milky Way we generate 100 Monte Carlo merger trees in 5 equally spaced bins of final halo masses in the range $5 \times 10^{11}\,M_\odot \leqslant M_{\rm halo}^{\rm host} \leqslant 2 \times 10^{12}\,M_\odot$. The cumulative V-band satellite luminosity functions at $z = 0$ are shown in Fig. 7 for our various dark matter models with the EvoFb feedback scheme. Before we attempt to compare these predictions with observations we note that the two different observational datasets plotted in the figure disagree with one another at the bright end of the luminosity function ($M_{\rm V} \leqslant -8$), which is the regime of the 11 "classical" satellites. There are two reasons for this difference: firstly, McConnachie (2012), whose measurements are included in the bright end of the 'Combined data' sample includes Canis Major ($M_{\rm V} = -14.4$), whereas this galaxy is excluded by Tollerud et al. (2008). Secondly, Tollerud et al. (2008) adopt $M_{\rm V} = -9.8$ for Sculptor, compared to McConnachie's value of $M_{\rm V} = -11.1$. At the faint end the differences in the satellite luminosity function arise from differing assumptions for the radial distributions of the satellites. In particular, Koposov et al. (2008) assume that the satellite distribution follows the NFW profile (Navarro et al. 1996, 1997) of the host halo, whereas Tollerud et al. (2008) assume the subhalo radial distribution measured in the Via Lactea simulations (Diemand et al. 2007). The radial distribution of subhaloes is similar in CDM and WDM (Bose et al. 2016a).

Fig. 7 shows that all of our models, including the most extreme $L_6 = 700$ case, are consistent with the data down to $M_{\rm V} \sim -5$. For CDM the EvoFb model slightly overpredicts the number of the faintest satellites ($M_{\rm V} > -8$), but here the data could be incomplete. However, since the number of satellites scales with the host halo mass (Wang et al. 2012; Cautun et al. 2014), our sterile neutrino models would be increasingly in conflict with the observed luminosity functions for $M_{\rm halo}^{\rm host} \leqslant 10^{12}\,M_\odot$. For example, if $M_{\rm halo}^{\rm host} \leqslant 7 \times 10^{11}\,M_\odot$, both the $L_6 = 700$ and $L_6 = 12$ EvoFb models would be ruled out because they fail to form enough faint satellites with $M_{\rm V} > -10$ even after accounting for the large scatter. Only CDM and our $L_6 = 8$ sterile neutrino models would remain consistent with the Koposov et al. (2008) and McConnachie (2012) ('Combined data') observations in this case.

The Dark Energy Survey (DES) recently reported the discovery of new ultra-faint dwarf galaxies (Bechtol et al. 2015; Koposov et al. 2015; Drlica-Wagner et al. 2015; Jethwa et al. 2016). We can consider their contribution to the observed luminosity function following the analysis by Jethwa et al. (2016) who find that 12 of the 14 satellites have $> 50\%$ probability of having been brought in as satellites of the LMC itself (at 95% confidence). Extrapolating from the detected population Jethwa et al. (2016) conclude that the Milky Way should have ~ 180 satellites within 300 kpc and 70^{+30}_{-40} Magellanic satellites in the magnitude range $-7 < M_{\rm V} < -1$ (at 68% confidence).

The extrapolated contribution of the DES satellites (a total of 250 satellites) is represented by the black diamond in Fig. 7. CDM is consistent with this number particularly for the larger assumed values of the mass of the Milky Way halo. On the other hand, the 'coldest' 7 keV sterile neutrino, namely $L_6 = 8$, is only marginally consistent with the extrapolation, while the $L_6 = 12$ and $L_6 = 700$ models are in significant disagreement with the extrapolated number count. The predicted number of faint dwarfs produced by any of these models is, of course, sensitive to the details of the SNfb but in the following section we consider a limiting case.

4.5 Model independent constraints on dark matter

As mentioned in Section 4.4 our analysis suffers from a degeneracy between the shape of the initial power spectrum and the strength of SNfb. A model independent constraint, however, can be derived by assuming that there is no SNfb at all. In this case, every subhalo in which gas can cool hosts a satellite, thus maximising the size of the population. In Fig. 8 we show the predicted Milky Way satellite luminosity function in the case of zero feedback ('NoFb'). The total number of satellites is determined entirely by reionisation i.e., by the amount of gas cooling in haloes prior to the onset of reionisation.

In Fig. 8 we have assumed $z_{\rm reion}^{\rm full} = 7.02$, as predicted by the EvoFb scheme for the $L_6 = 8$ model. This produces, on average, ~ 100 satellites with $M_{\rm V} \leqslant -1$. A fully self-consistent treatment of reionisation for the NoFb model would result in $z_{\rm reion}^{\rm full} > 7.02$, in which case the number of satellites produced would be even less than 100. The maximum number of satellite galaxies produced in Fig. 8 is converged with respect to the halo mass resolution. The figure shows that the extreme NoFb model is only marginally consistent with the extrapolated DES data for the $L_6 = 8$ case. We recall that this value of the lepton asymmetry corresponds to the 'coldest' possible 7 keV sterile neutrino; ruling this out would rule out the entire family of 7 keV sterile neutrinos as the dark matter particles.

The exact location of the extrapolated DES data point in the cumulative luminosity function is subject to a number of caveats, such as the DES selection function, detection efficiency and assumptions about isotropy. However, it is clear that the discovery

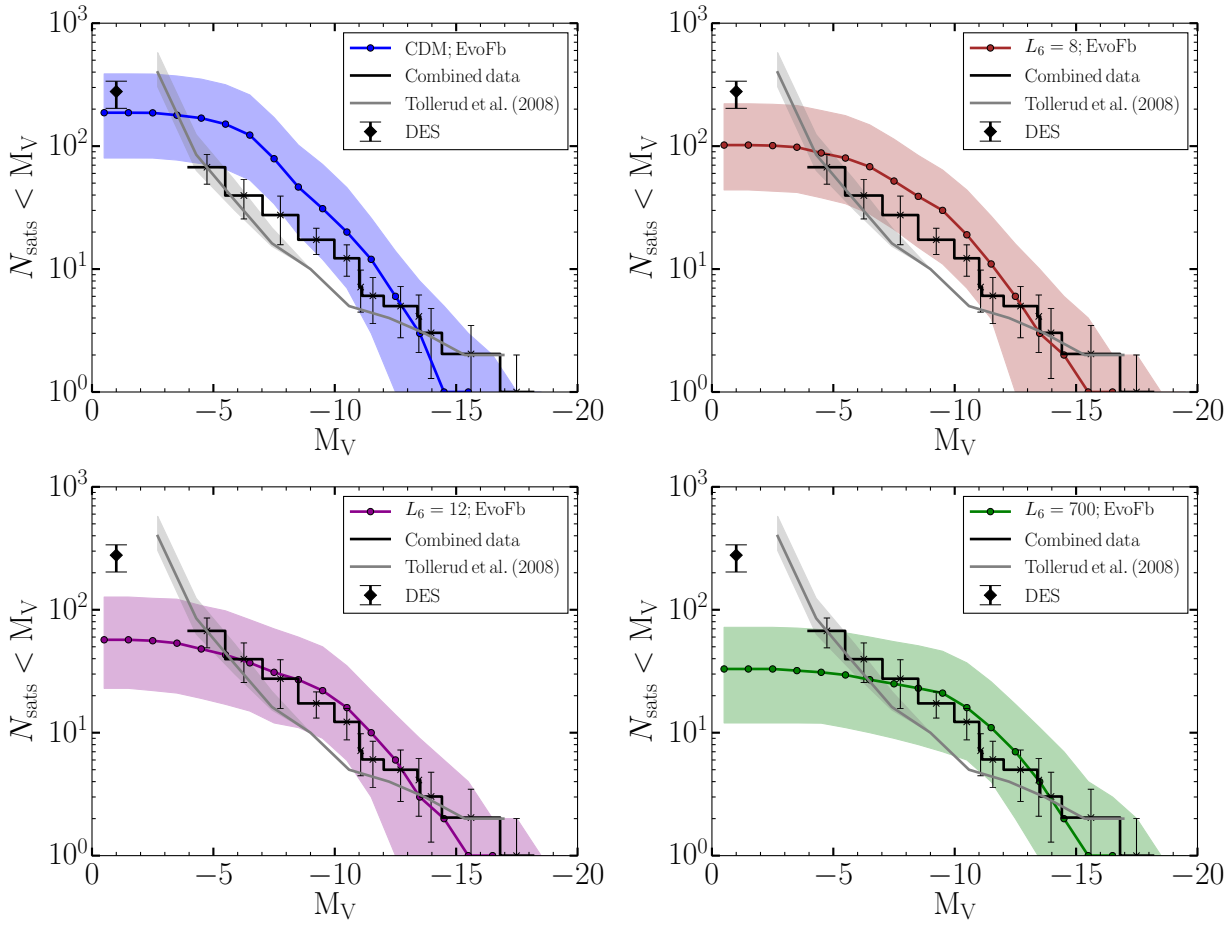

Figure 7. Cumulative V-band Milky Way satellite luminosity functions at $z = 0$ for our four dark matter models with EvoFb supernova feedback. In each case, we have used 100 Monte Carlo merger trees for haloes of final mass in the range $5 \times 10^{11} - 2 \times 10^{12}\,M_{\odot}$. The smooth solid line indicates the median and the coloured shaded region the 5th and 95th percentiles over all realisations. The black histogram labelled 'Combined data' shows the observed Milky Way satellite luminosity function obtained by combining two datasets: for $M_{\rm V} \geqslant -11$ the data are taken from Koposov et al. (2008), which includes corrections for incompleteness in the SDSS DR5 catalogue; for $M_{\rm V} < -11$, the data are taken from McConnachie (2012). The solid grey line shows the satellite luminosity function from Tollerud et al. (2008) with the grey shaded region showing the 98% spread over 18,576 mock surveys of the Milky Way halo in the Via Lactea simulation (Diemand et al. 2007). The black diamond marks an extension of the observed satellite luminosity function adding the new ultra-faint dwarf satellites discovered by DES down to $M_{\rm V} \leqslant -1$ (Jethwa et al. 2016). The partial sky coverage of the survey is taken into account. All error bars are Poisson errors, including volume corrections where appropriate.

of even more ultra-faint dwarf galaxies could potentially set very strong constraints on the nature of the dark matter.

5 CONCLUSIONS

We have carried out a detailed investigation of the process of reionisation in models in which the dark matter particles are assumed to be sterile neutrinos. The free streaming of these particles leads to a sharp cut-off in the primordial matter power spectrum at the scale of dwarf galaxies (Section 2, Fig. 1). On scales much larger than the cut-off, structure formation proceeds almost identically to CDM. Near and below the cut-off, sterile neutrinos behave like warm dark matter (WDM): the abundance of haloes (and therefore of the galaxies they host) is suppressed and their formation times are delayed relative to CDM. The sterile neutrino models we consider are motivated by observations of an X-ray excess at 3.5 keV in the stacked spectrum of galaxy clusters (Bulbul et al. 2014) and in the spectra of M31 and the Perseus cluster (Boyarsky et al. 2014).

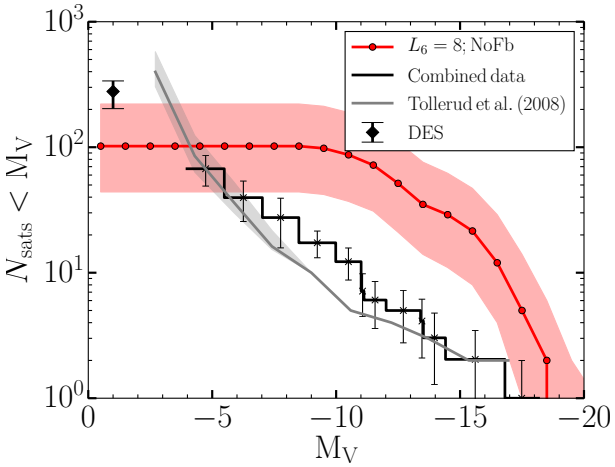

Figure 8. Same as Fig. 7 for the $L_6 = 8$ model, but in an extreme scenario where feedback has been turned off completely.

This excess could be explained by the decay of a sterile neutrino with a rest mass of 7 keV.

In addition to their rest mass, sterile neutrinos are characterised by two additional parameters: the lepton asymmetry, L_6, and the mixing angle. Keeping the mass of the sterile neutrino fixed at 7 keV, we consider three values of L_6: 8, 12, 700. Based on their cut-off scales, the $L_6 = 8$ and $L_6 = 12$ models respectively correspond to the 'coldest' and 'warmest' 7 keV sterile neutrinos that are also consistent with the Bulbul et al. (2014) and Boyarsky et al. (2014) observations. The most extreme model we consider, $L_6 = 700$, also decays at 3.5 keV but the mixing angle is unable to produce a decay flux compatible with the 3.5 keV X-ray observations (see Table 1 for a summary).

To calculate the number of ionising photons produced in CDM and in the sterile neutrino models, we make use of the Durham semi-analytic model of galaxy formation, GALFORM using the supernova feedback prescription of Hou et al. (2015). In this model, the parameters controlling the strength and evolution of supernova feedback are calibrated for CDM by the epoch of reionisation as measured by *Planck*, and tested against data for the luminosity function and stellar mass-metallicity relation of Milky Way satellites (Section 3.2). We adopt similar values of the model parameters for our sterile neutrino models. Our main conclusions are:

(i) Although reionisation occurs slightly later in the sterile neutrino models than in CDM, the epoch of reionisation in all cases is consistent with the bounds from *Planck* (Section 4.2, Fig. 4). For the $L_6 = (12, 700)$ models, the redshifts at which the Universe is 50% ionised are just below the 68% confidence interval from *Planck*. Reionisation in the $L_6 = 8$ model occurs well within the *Planck* limits.

(ii) The galaxies that account for the bulk of the ionising photon budget are more massive in sterile neutrino models than in CDM (Section 4.3, Fig. 5). By the time reionisation is complete, 50% of the photoionising budget is produced by $M_\star \lesssim 10^8\, M_\odot$ galaxies in CDM; the median stellar mass is $M_\star \sim 10^9\, M_\odot$ for the sterile neutrino models.

(iii) From the evolution of the far-UV luminosity function, we infer that the galaxy population at high redshift ($z > 7$) builds up more rapidly in the sterile neutrino models than in CDM (Section 4.3, Fig. 6). This is particularly pronounced in the case of the most extreme model, $L_6 = 700$, which produces far fewer galaxies than CDM at $z = 10$ but 'catches up' with the CDM UV luminosity function by $z = 7$. This is directly related to the more rapid mass accretion of haloes near the free streaming scale in WDM than in CDM. The qualitative difference in the growth of high redshift galaxies between CDM and WDM models does not depend on the details of the galaxy formation model.

(iv) CDM, as well as the three sterile neutrino models we have considered, are in good agreement with the present-day luminosity function of the "classical" and SDSS Milky Way satellite galaxies (Section 4.4, Fig. 7). For larger values of the mass of the Milky Way halo ($M_{\rm halo}^{\rm host} > 1 \times 10^{12} M_\odot$), even the $L_6 = 700$ model is consistent with the observations of Koposov et al. (2008) and McConnachie (2012). On the other hand, if $M_{\rm halo}^{\rm host} \leqslant 7 \times 10^{11} M_\odot$, both the $L_6 = 700$ and $L_6 = 12$ models can be ruled out.

(v) Extrapolating to the whole sky the abundance of ultra-faint Milky Way dwarf satellite galaxies recently detected by DES extends that satellite luminosity function to very faint magnitudes. With this extrapolation, the sheer number of satellites places strong constraints on the sterile neutrino models which produce only a limited number of substructures. CDM is consistent with this extrapolation, but the 'coldest' 7 keV sterile neutrino (the $L_6 = 8$ model) is only marginally in agreement even when feedback is turned off completely, a limiting model in which the satellite population is maximised. Ruling out the $L_6 = 8$ model, the coolest of the 7keV sterile neutrino family, would rule out this entire class as candidates for the dark matter. However, extrapolating the DES counts to infer the total number of satellites is still subject to a number of assumptions and uncertainties.

The largest observable differences between CDM and sterile neutrino models occur at the scale of ultra-faint dwarfs and galaxies at high redshift. However, only limited data are currently available in these regimes. The gravitational lensing techniques pioneered by Koopmans (2005) and Vegetti & Koopmans (2009) may be used to constrain the subhalo mass function directly, potentially distinguishing WDM from CDM (Li et al. 2015). By increasing the sample of strong lensing systems, upcoming telescopes such as the SKA and LSST could play a major role in constraining the nature of the dark matter.

ACKNOWLEDGEMENTS

We would like to thank Mikko Laine, Alexey Boyarsky and Oleg Ruchayskiy for providing us with the codes for generating the sterile neutrino power spectra. SB is supported by STFC through grant ST/K501979/1. This work was supported in part by ERC Advanced Investigator grant COSMIWAY [grant number GA267291] and the Science and Technology Facilities Council [grant number ST/F001166/1, ST/I00162X/1]. This work used the DiRAC Data Centric system at Durham University, operated by the Institute for Computational Cosmology on behalf of the STFC DiRAC HPC Facility (www.dirac.ac.uk). This equipment was funded by BIS National E-infrastructure capital grant ST/K00042X/1, STFC capital grant ST/H008519/1, and STFC DiRAC Operations grant ST/K003267/1 and Durham University. DiRAC is part of the National E-Infrastructure. This research was carried out with the support of the HPC Infrastructure for Grand Challenges of Science and Engineering Project, co-financed by the European Regional Development Fund under the Innovative Economy Operational Programme. The data analysed in this paper can be made available upon request to the author.

REFERENCES

Abazajian K. N., 2014, Physical Review Letters, 112, 161303
Abazajian K., Fuller G. M., Patel M., 2001a, Phys. Rev. D, 64, 023501
Abazajian K., Fuller G. M., Tucker W. H., 2001b, ApJ, 562, 593
Ade P. A. R., et al., 2015, preprint, (arXiv:1502.01589)
Anderson M. E., Churazov E., Bregman J. N., 2015, MNRAS, 452, 3905
Asaka T., Shaposhnikov M., 2005, Physics Letters B, 620, 17
Asaka T., Shaposhnikov M., Laine M., 2007, Journal of High Energy Physics, 1, 91
Avila-Reese V., Colín P., Valenzuela O., D'Onghia E., Firmani C., 2001, ApJ, 559, 516
Baugh C. M., Lacey C. G., Frenk C. S., Granato G. L., Silva L., Bressan A., Benson A. J., Cole S., 2005, MNRAS, 356, 1191
Baur J., Palanque-Delabrouille N., Yèche C., Magneville C., Viel M., 2015, preprint, (arXiv:1512.01981)
Bechtol K., et al., 2015, ApJ, 807, 50
Benson A. J., Frenk C. S., Baugh C. M., Cole S., Lacey C. G., 2003, MNRAS, 343, 679
Benson A. J., et al., 2013, MNRAS, 428, 1774
Bode P., Ostriker J. P., Turok N., 2001, ApJ, 556, 93

Bose S., Hellwing W. A., Frenk C. S., Jenkins A., Lovell M. R., Helly J. C., Li B., Gao L., 2016a, preprint, (arXiv:1604.07409)
Bose S., Hellwing W. A., Frenk C. S., Jenkins A., Lovell M. R., Helly J. C., Li B., 2016b, MNRAS, 455, 318
Bouwens R. J., et al., 2011a, Nature, 469, 504
Bouwens R. J., et al., 2011b, ApJ, 737, 90
Bouwens R. J., et al., 2015, ApJ, 803, 34
Bower R. G., Benson A. J., Malbon R., Helly J. C., Frenk C. S., Baugh C. M., Cole S., Lacey C. G., 2006, MNRAS, 370, 645
Bowler R. A. A., et al., 2014, MNRAS, 440, 2810
Boyarsky A., Lesgourgues J., Ruchayskiy O., Viel M., 2009a, J. Cosmology Astropart. Phys., 5, 012
Boyarsky A., Ruchayskiy O., Shaposhnikov M., 2009b, Annual Review of Nuclear and Particle Science, 59, 191
Boyarsky A., Lesgourgues J., Ruchayskiy O., Viel M., 2009c, Physical Review Letters, 102, 201304
Boyarsky A., Ruchayskiy O., Iakubovskyi D., Franse J., 2014, Physical Review Letters, 113, 251301
Bozek B., Boylan-Kolchin M., Horiuchi S., Garrison-Kimmel S., Abazajian K., Bullock J. S., 2016, MNRAS, 459, 1489
Bulbul E., Markevitch M., Foster A., Smith R. K., Loewenstein M., Randall S. W., 2014, ApJ, 789, 13
Calura F., Menci N., Gallazzi A., 2014, MNRAS, 440, 2066
Canetti L., Drewes M., Shaposhnikov M., 2013, Physical Review Letters, 110, 061801
Cautun M., Frenk C. S., van de Weygaert R., Hellwing W. A., Jones B. J. T., 2014, MNRAS, 445, 2049
Cole S., Aragon-Salamanca A., Frenk C. S., Navarro J. F., Zepf S. E., 1994, MNRAS, 271, 781
Cole S., Lacey C. G., Baugh C. M., Frenk C. S., 2000, MNRAS, 319, 168
Cole S., et al., 2005, MNRAS, 362, 505
Colín P., Avila-Reese V., Valenzuela O., 2000, ApJ, 542, 622
Colín P., Avila-Reese V., González-Samaniego A., Velázquez H., 2015, ApJ, 803, 28
Dayal P., Choudhury T. R., Bromm V., Pacucci F., 2015a, preprint, (arXiv:1501.02823)
Dayal P., Mesinger A., Pacucci F., 2015b, ApJ, 806, 67
Diemand J., Kuhlen M., Madau P., 2007, ApJ, 657, 262
Dodelson S., Widrow L. M., 1994, Physical Review Letters, 72, 17
Dolgov A. D., Hansen S. H., 2002, Astroparticle Physics, 16, 339
Driver S. P., et al., 2012, MNRAS, 427, 3244
Drlica-Wagner A., et al., 2015, ApJ, 813, 109
Efstathiou G., 1992, MNRAS, 256, 43P
Eisenstein D. J., et al., 2005, ApJ, 633, 560
Finkelstein S. L., et al., 2014, preprint, (arXiv:1410.5439)
Finlator K., Oh S. P., Özel F., Davé R., 2012, MNRAS, 427, 2464
Garzilli A., Boyarsky A., Ruchayskiy O., 2015, preprint, (arXiv:1510.07006)
Ghiglieri J., Laine M., 2015, Journal of High Energy Physics, 11, 171
Gonzalez-Perez V., Lacey C. G., Baugh C. M., Lagos C. D. P., Helly J., Campbell D. J. R., Mitchell P. D., 2014, MNRAS, 439, 264
Governato F., et al., 2015, MNRAS, 448, 792
Hooper D., Goodenough L., 2011, Physics Letters B, 697, 412
Hou J., Frenk C. S., Lacey C. G., Bose S., 2015, preprint, (arXiv:1512.04595)
Iliev I. T., Mellema G., Pen U.-L., Merz H., Shapiro P. R., Alvarez M. A., 2006, MNRAS, 369, 1625
Jeltema T. E., Profumo S., 2015a, preprint, (arXiv:1512.01239)
Jeltema T., Profumo S., 2015b, MNRAS, 450, 2143
Jenkins A., Frenk C. S., White S. D. M., Colberg J. M., Cole S., Evrard A. E., Couchman H. M. P., Yoshida N., 2001, MNRAS, 321, 372
Jethwa P., Erkal D., Belokurov V., 2016, preprint, (arXiv:1603.04420)
Kauffmann G., White S. D. M., Guiderdoni B., 1993, MNRAS, 264, 201
Kennedy R., Frenk C., Cole S., Benson A., 2014, MNRAS, 442, 2487
Khaire V., Srianand R., Choudhury T. R., Gaikwad P., 2016, MNRAS, 457, 4051
Koopmans L. V. E., 2005, MNRAS, 363, 1136
Koposov S., et al., 2008, ApJ, 686, 279
Koposov S. E., Belokurov V., Torrealba G., Evans N. W., 2015, ApJ, 805, 130
Lacey C. G., et al., 2015, preprint, (arXiv:1509.08473)
Lagos C. D. P., Lacey C. G., Baugh C. M., Bower R. G., Benson A. J., 2011, MNRAS, 416, 1566
Lagos C. d. P., Lacey C. G., Baugh C. M., 2013, MNRAS, 436, 1787
Laine M., Shaposhnikov M., 2008, J. Cosmology Astropart. Phys., 6, 31
Larson R. B., 1974, MNRAS, 169, 229
Lewis A., Challinor A., Lasenby A., 2000, ApJ, 538, 473
Li R., Frenk C. S., Cole S., Gao L., Bose S., Hellwing W. A., 2015, preprint, (arXiv:1512.06507)
Lovell M. R., et al., 2012, MNRAS, 420, 2318
Lovell M. R., Frenk C. S., Eke V. R., Jenkins A., Gao L., Theuns T., 2014, MNRAS, 439, 300
Lovell M. R., et al., 2015, preprint, (arXiv:1511.04078)
Ludlow A. D., Bose S., Angulo R. E., Wang L., Hellwing W. A., Navarro J. F., Cole S., Frenk C. S., 2016, preprint, (arXiv:1601.02624)
Macciò A. V., Fontanot F., 2010, MNRAS, 404, L16
Madau P., Haardt F., 2015, ApJ, 813, L8
Maio U., Viel M., 2015, MNRAS, 446, 2760
Malyshev D., Neronov A., Eckert D., 2014, Phys. Rev. D, 90, 103506
McConnachie A. W., 2012, AJ, 144, 4
McLure R. J., et al., 2013, MNRAS, 432, 2696
Mitra S., Choudhury T. R., Ferrara A., 2015, MNRAS, 454, L76
Navarro J. F., Frenk C. S., White S. D. M., 1996, ApJ, 462, 563
Navarro J. F., Frenk C. S., White S. D. M., 1997, ApJ, 490, 493
Nierenberg A. M., Treu T., Menci N., Lu Y., Wang W., 2013, ApJ, 772, 146
Norberg P., et al., 2002, MNRAS, 336, 907
Oesch P. A., et al., 2012, ApJ, 759, 135
Oesch P. A., et al., 2014, ApJ, 786, 108
Okamoto T., Gao L., Theuns T., 2008, MNRAS, 390, 920
Parkinson H., Cole S., Helly J., 2008, MNRAS, 383, 557
Polisensky E., Ricotti M., 2011, Phys. Rev. D, 83, 043506
Raičević M., Theuns T., Lacey C., 2011, MNRAS, 410, 775
Riemer-Sorensen S., 2014, preprint, (arXiv:1405.7943)
Robertson B. E., Ellis R. S., Furlanetto S. R., Dunlop J. S., 2015, ApJ, 802, L19
Ruchayskiy O., et al., 2015, preprint, (arXiv:1512.07217)
Rudakovskiy A., Iakubovskyi D., 2016, preprint, (arXiv:1604.01341)
Sawala T., et al., 2015, MNRAS, 448, 2941
Schenker M. A., et al., 2013, ApJ, 768, 196
Schneider A., 2016, preprint, (arXiv:1601.07553)
Schneider A., Smith R. E., Macciò A. V., Moore B., 2012, MNRAS, 424, 684
Schultz C., Oñorbe J., Abazajian K. N., Bullock J. S., 2014, MNRAS, 442, 1597
Sharma M., Theuns T., Frenk C., Bower R., Crain R., Schaller M., Schaye J., 2016, MNRAS,
Sheth R. K., Tormen G., 1999, MNRAS, 308, 119
Shi X., Fuller G. M., 1999, Physical Review Letters, 82, 2832
Tinker J., Kravtsov A. V., Klypin A., Abazajian K., Warren M., Yepes G., Gottlöber S., Holz D. E., 2008, ApJ, 688, 709
Tollerud E. J., Bullock J. S., Strigari L. E., Willman B., 2008, ApJ, 688, 277
Trac H., Cen R., 2007, ApJ, 671, 1
Vegetti S., Koopmans L. V. E., 2009, MNRAS, 400, 1583
Venumadhav T., Cyr-Racine F.-Y., Abazajian K. N., Hirata C. M., 2015, preprint, (arXiv:1507.06655)
Viel M., Lesgourgues J., Haehnelt M. G., Matarrese S., Riotto A., 2005, Phys. Rev. D, 71, 063534
Viel M., Becker G. D., Bolton J. S., Haehnelt M. G., 2013, Phys. Rev. D, 88, 043502
Wang J., White S. D. M., 2007, MNRAS, 380, 93
Wang J., Frenk C. S., Navarro J. F., Gao L., Sawala T., 2012, MNRAS, 424, 2715
White S. D. M., Frenk C. S., 1991, ApJ, 379, 52
Zehavi I., et al., 2011, ApJ, 736, 59